Molecular-Scale Characterization of the Reaction of Ozone with Decanethiol Monolayers on Au(111)

Gregory E. Poirier,* Tonya M. Herne, C. Cameron Miller, and Michael J. Tarlov

Contribution from the National Institute of Standards and Technology, Gaithersburg, Maryland 20899

Received May 25, 1999

Abstract: The chemical reaction of ozone with decanethiol monolayers on Au(111) was characterized using X-ray photoelectron spectroscopy and scanning tunneling microscopy. Our results show that exposure to ozone results in oxidation of the thiol terminus. The reaction initiates at the domain boundary network of the alkanethiol monolayer and propagates into the domains. Above a threshold surface oxygen content, the monolayer converts to a two-dimensional fluid that can subsequently recrystallize to a commensurate monolayer of partially oxidized thiol. Further exposure to ozone results in conversion of the monolayer to a fluid phase and a 10% to 30% expansion of the Au lattice at the Au−thiol interface with concomitant formation of Au islands. Our results demonstrate that crystallographic defects in monolayer films can play an important role in their chemical reactions.

Introduction

Alkanethiol monolayers on Au(111)[1,2] have served as a model system for fundamental studies of biological membranes,[3−5] of corrosion,[6] of wetting,[7] and of monolayer lithography.[8,9] Though extremely useful in these fundamental studies, practical questions must be addressed if these systems are to successfully transfer to commercial applications, questions such as: What is the expected shelf life of alkanethiol monolayers? and With what ambient air species do the monolayers react? Early studies suggested that monolayers may be less than 2% oxidized by exposure to air;[10,11] more recent studies indicate nearly complete oxidation of alkanethiol monolayers in air.[12−15] The chemical composition of air includes several oxygen containing species: O_2, H_2O, CO_2, O_3, OH radical, and other components.[16] The weight of the evidence indicates that the dominant species resulting in monolayer oxidation is ozone.[12,17,18] Reports on the rate of oxidation in air have varied widely from hours,[14] to days,[10−13] to months;[15] these discrepancies possibly result from local variations in ambient ozone level, from variations in monolayer storage conditions, and from chain-length-dependence of the reaction rate.[10,12] What remains unknown is the site of attack and the nature and extent of morphological changes accompanying oxidation. Knowledge of the point of attack and path of progression may provide the insight to design more robust monolayers. The goal of this paper is to provide a molecular-scale picture of the morphological changes accompanying ozone-induced oxidation of alkanethiol monolayers on Au(111). We begin with a brief description of our experimental apparatus and procedure. This is followed by characterization of the purity of our ozone source. Next we discuss photoelectron spectroscopy data that correlate chemical reactions occurring in air with those occurring in ozone. This is followed by a discussion of scanning tunneling microscopy data that reveal molecular-scale morphological changes accompanying the ozone-induced oxidation.

Experimental Section

Apparatus and Substrate. Studies were conducted on well-characterized single-crystal Au(111) surfaces in the well-controlled environment of an ultrahigh vacuum (UHV) chamber. The system has a base pressure of 3×10^{-8} Pa (2×10^{-10} Torr) and is equipped with a rapid-entry load-lock. Quadrupole mass spectroscopy data were acquired using a commercially available instrument operated at 40 eV ionization energy and 0.75 mA emission current. X-ray photoelectron spectroscopy (XPS) data were acquired using a commercially available instrument with a Mg anode operated at 12 kV and 20 mA. Spectra were acquired from binding energy regions in the following order: O 1*s*, S 2*p*, C 1*s*, and Au 4*f*, followed by a survey scan from 1000 to 10 eV to check for contaminants. Reproducibility of the XPS data was confirmed by measuring XPS data on three different samples of nascent thiolate monolayer, seven different samples of those exposed to ozone in vacuo, and four different samples of those exposed to air. Acquisition

(1) Poirier, G. E. *Chem. Rev.* **1997**, *97*, 1117−1127.
(2) Ulman, A. *Chem. Rev.* **1996**, *96*, 1533−1554.
(3) Plant, A. L. *Langmuir* **1993**, *9*, 2764−2767.
(4) Lang, H.; Duschl, C.; Gratzel, M.; Vogel, H. *Thin Solid Films* **1992**, *210/211*, 818−821.
(5) Lingler, S.; Rubenstein, I.; Knoll, W.; Offenhausser, A. *Langmuir* **1997**, *13*, 7085−7091.
(6) Chailapakul, O.; Sun, L.; Xu, C.; Crooks, R. M. *J. Am. Chem. Soc.* **1993**, *115*, 12459−12467.
(7) Olbris, D. J.; Ulman, A.; Shnidman, Y. *J. Phys. Chem.* **1995**, *99*, 6865−6873.
(8) Wilbur, J. L.; Biebuyck, H. A.; MacDonald, J. C.; Whitesides, G. M. *Langmuir* **1995**, *11*, 825−831.
(9) Bernard, A.; Delamarche, E.; Schmid, H.; Michel, B.; Bosshard, H. R.; Biebuyck, H. *Langmuir* **1998**, *14*, 2225−2229.
(10) Li, Y.; Huang, J.; Robert T. McIver, J.; Hemminger, J. C. *J. Am. Chem. Soc.* **1992**, *114*, 2428−2432.
(11) Tarlov, M. J.; Newman, J. G. *Langmuir* **1992**, *8*, 1398−1405.
(12) Schoenfisch, M. H.; Pemberton, J. E. *J. Am. Chem. Soc.* **1998**, *120*, 4502−4513.
(13) Lee, M.-T.; Hsueh, C.-C.; Freund, M. S.; Ferguson, G. S. *Langmuir* **1998**, *14*, 6419−6423.
(14) Scott, J. R.; Baker, L. S.; Everett, W. R.; Wilkins, C. L.; Fritsch, I. *Anal. Chem.* **1997**, *69*, 2636−2639.
(15) Horn, A. B.; Russell, D. A.; Shorthouse, L. J.; Simpson, T. R. E. *J. Chem. Soc., Faraday Trans.* **1996**, *92*, 4759−4762.
(16) Seinfeld, J. H. *Atmospheric Chemistry and Physics of Air Pollution*; J. Wiley: New York, 1986.
(17) Zhang, Y.; Terrill, R. H.; Tanzer, T. A.; Bohn, P. W. *J. Am. Chem. Soc.* **1998**, *120*, 2654−2655.
(18) Norrod, K. L.; Rowlen, K. L. *J. Am. Chem. Soc.* **1998**, *120*, 2656−2657.

10.1021/ja991739f
Published on Web 09/29/1999

of the four binding energy windows and the survey scan required a total exposure time of 30−40 min. Propensity of the X-ray beam to modify the monolayers was checked by looking for a change in the O 1*s* intensity following the 30−40 min exposure and by measuring topography using STM before and after 30−40 min exposure to X-rays. Nascent thiolate monolayers exhibited no detectable oxygen (and no variation with exposure time) and no detectable change in surface topograph following X-ray exposure. Oxidized thiol monolayers showed no detectable change in O 1*s* signal following X-ray exposure, however, STM revealed X-ray induced morphological changes in the form of a redispersion of island features created during oxidation. Scanning tunneling microscopy (STM) data were acquired using a custom-built instrument operated at a constant tunneling current between 10 to 100 pA and tunneling bias between ±(0.5−1.5) V. Our substrate was a Au(111) single crystal obtained from Bud Addis at Cornell University (typical purity 99.999%).[19] The crystal surface was cleaned by Ar^+ sputtering at 500 eV, 2 μA, and subsequent annealing at 500−600 °C for 10 min. Surface purity was confirmed using XPS and STM.

Monolayer Preparation. Solutions of decanethiol (97% purity, 1.0 mM) in ethanol (200 proof, Warner-Graham Co.[19]) were prepared and stored in glass-sealed volumetric flasks. Monolayers were prepared by placing the clean Au(111) crystal in a cleaned glass incubation dish with a ground glass seal, adding 3−4 mL of decanethiol solution, covering, and incubating overnight (12−14 h). The crystal was then removed from the incubation bath, rinsed under a stream of 200 proof ethanol from a squeeze bottle (2−4 mL of ethanol were consumed in the rinse), and dried under a stream of dry nitrogen (5−10 s).[20] With the exception of growth-rate dependent variations in domain size, monolayer samples prepared in this manner were structurally indistinguishable (as measured by STM) and chemically indistinguishable (as measured by XPS) from those prepared by vacuum deposition of purified decanethiol.[21] Samples intended for controlled exposure to ozone were transferred to our UHV system via a rapid-entry load-lock with less than 15 min exposure to air. Samples intended for exposure to laboratory air were placed in an open fluoroware container on a lab bench. A cylindrical card-stock container with a loose fitting lid was placed over the samples to allow air access but inhibit dust accumulation.

Ozone Preparation. Ozone was generated using a generator from PCI Ozone Corporation[19] by passing molecular oxygen through a 70 VAC discharge. The ozone was collected on dry silica gel beads, 1−3 mm in diameter, packed in a glass vessel which itself was packed in dry ice. The temperature measured on the outside of the vessel varied from −70 to −80 °C. Adsorption of ozone causes a color change of the silica gel from white to azure. The vessel inlet and outlet were sealed by Teflon needle valves and the vessel was connected to the UHV system using a variable leak valve. ***We caution the reader that a severe explosion hazard results if the ozone-saturated silica gel in the glass vessel is allowed to warm close to room temperature.***[22] At the end of the experiments, ozone was removed from the silica gel by controlled pumping of the headspace volume with a mechanical pump lubricated by perfluorinated oil.

Results and Discussion

Prior to performing the monolayer oxidation experiments, the species comprising the headspace volume of the ozone-saturated silica gel vessel were characterized using mass spectrometry (MS). MS of the vessel headspace immediately after its removal from the ozone generator revealed molecular oxygen as the primary component. Evacuation of the headspace for ∼15 min by a turbomolecular pump lowered the partial pressure of O_2 to the point where ozone became the dominant species. The mass spectrum of the purified vessel headspace (at 1×10^{-6} Pa (1×10^{-8} Torr)) is compared to the mass spectrum of the chamber background gas in Figure 1. Peaks at 48, 32, and 16 amu are attributed to O_3^+ and its cracking fragments O_2^+ and O^+. Intensity at 32 and 16 amu may be partly due to molecular oxygen from spontaneous decomposition of ozone in the vessel. The spectrum also indicates mass peaks at 44, 28, and 18 amu. We attribute these to CO_2^+, its cracking fragment (CO^+), and water. Both species may have frozen on the silica gel during the trapping process and subsequently sublimated into the vessel headspace. We conclude, therefore, that the vessel headspace comprises ozone and several other oxygen containing species.

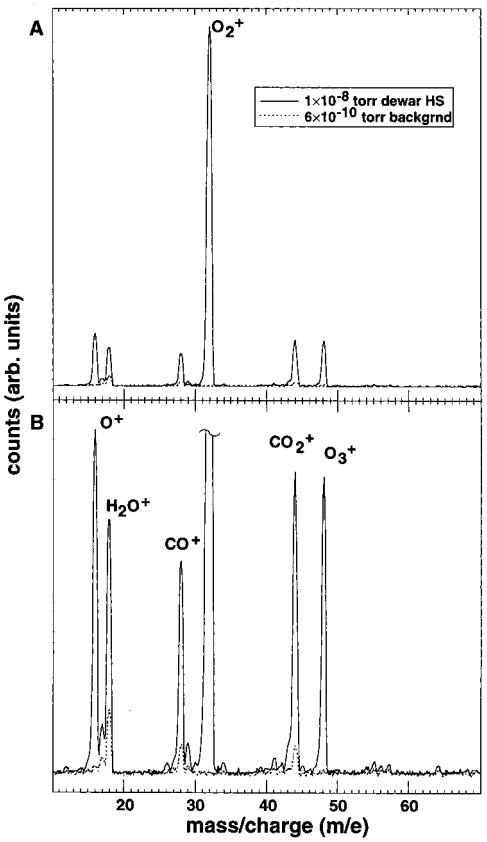

Figure 1. Quadrupole mass spectrum of residual chamber gases (dotted lines) (at 7×10^{-8} Pa (5×10^{-10} Torr)) and of the headspace gas of the ozone saturated silica gel on dry ice (solid lines) (at 1×10^{-6} Pa (1×10^{-8} Torr)). Spectra are shown full scale in (A) and expanded scale in (B). Spectra confirm the presence of ozone and reveal residual contaminant gases including H_2O and CO_2.

XPS was used to measure the change in surface chemical composition following exposure of the decanethiol monolayers to air and to the vessel headspace. All of the photoemission peaks in a survey scan could be attributed to either the Au surface or to the alkanethiol monolayer. Photoemission spectra of the O 1*s* binding energy region (Figure 2A) indicate that thiolate monolayers that are exposed to laboratory air for less than 15 min exhibit no detectable oxygen; however, exposure of thiolate monolayers to either laboratory air for 24 h or to 1×10^{-5} Pa (10^{-7} Torr) of the vessel headspace for 20 min results in appearance of an O 1*s* feature of comparable intensity. Photoemission spectra acquired from the S 2*p* binding energy region (Figure 2B) indicate that thiolate monolayers exposed to laboratory air for less than 15 min exhibit a S 2*p* binding

(19) The identification of commercial products and their sources is made to describe the experiment adequately. In no case does this identification imply recommendation by the National Institute of Standards and Technology, nor does it imply that the products are the best available.

(20) Nuzzo, R. G.; Allara, D. L. *J. Am. Chem. Soc.* **1983**, *105*, 4481−4483.

(21) Poirier, G. E. *Langmuir* **1999**, *15*, 1167−1175; see also: Poirier, G. E. *Langmuir* **1999**, *15*, 3018−3020.

(22) Saliba, N.; Parker, D. H.; Koel, B. E. *Surf. Sci.* **1998**, *410*, 270−282.

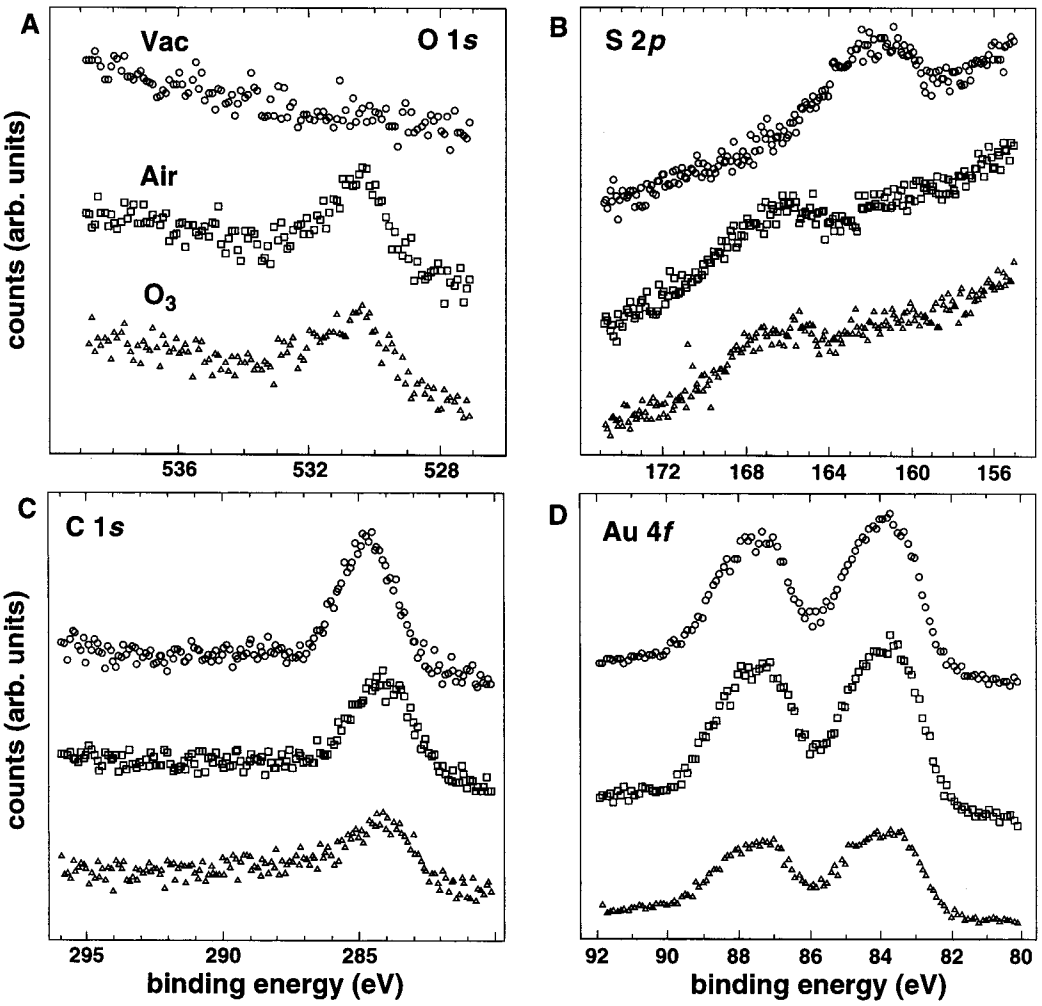

Figure 2. X-ray photoelectron spectra of nascent and oxidized decanethiol monolayers on Au(111) single crystal. All spectra were acquired from monolayers grown in 1 mM decanethiol in ethanol. Spectra in open circles are from sample exposed to laboratory air for less than 15 min (labeled "vac" in A) spectra in open squares are from sample exposed to laboratory air for 24 h (labeled "air" in A), spectra in open triangles are from sample exposed to laboratory air for less than 15 min then exposed to 10^{-5} Pa (10^{-7} Torr) of ozone vessel headspace for 20 min (labeled O_3 in A). (A) Spectra in O 1*s* region show that the monolayer exposed to air for less than 15 min contains less than detectable oxygen and monolayers exposed to air for 24 h or ozone have comparable oxygen content. (B) Spectra in S 2*p* region show that sulfur in nascent monolayer exists in reduced form, whereas monolayers exposed to either air or ozone exhibit binding energy shift consistent with oxidized sulfur and attenuation of the peak intensity. (C) Spectra in C 1*s* region show that monolayers exposed to either air or ozone exhibit loss of carbon intensity. (D) Spectra in Au 4*f* region show that monolayers exposed to either air or ozone exhibit broadening to higher binding energy and modulation of peak height.

energy consistent with reduced sulfur; however, exposure to either laboratory air for 24 h or to 1×10^{-5} Pa (10^{-7} Torr) of the vessel headspace for 20 min results in a binding energy shift to a value consistent with oxidized sulfur and a concomitant attenuation of photoelectron intensity.[12,23] Photoemission spectra acquired from the C 1*s* binding energy region (Figure 2C) indicate that thiolate monolayers exposed to laboratory air for 24 h exhibit a decrease in C 1*s* intensity and that monolayers exposed to 1×10^{-5} Pa (10^{-7} Torr) of the vessel headspace for 20 min result in a more pronounced decrease. Loss of intensity in both the S 2*p* and C 1*s* regions suggests that a fraction of the molecules desorb during oxidation of the monolayer; consistent with the report of Schoenfisch and Pemberton.[12] Photoemission spectra acquired from the Au 4*f* region (Figure 2D) indicate that thiolate monolayers exposed to laboratory air for 24 h exhibit an enhanced photoemission intensity with a slight broadening of peak width to higher binding energy. In contrast, monolayers exposed to 1×10^{-5} Pa (10^{-7} Torr) of the vessel headspace for 20 min exhibit attenuation of peak height and more pronounced broadening to higher binding energy. Broadening to higher binding energy is consistent with oxidation of the surface Au;[23] we do not have an explanation for the divergent behavior of the peak intensities. To summarize, consistent with the careful XPS studies of Schoenfisch and Pemberton,[12] our data indicate that exposure of decanethiolate monolayers to laboratory air for 24 h results in nearly complete oxidation of the sulfur termini and concomitant decrease in surface molecular density. Moreover, our data indicate that exposure to 1×10^{-5} Pa (10^{-7} Torr) of nominally pure ozone for 20 min results in comparable changes.[17,18]

To confirm that the other oxygen containing species in the vessel headspace (H_2O, CO_2, and O_2) are not the primary cause of the observed oxidation, the UHV chamber was filled to pressures of the pure components and monolayer samples were stored in the chamber. A monolayer sample was stored for 24 h in 1300 Pa (10 Torr) of H_2O vapor, another was stored for 22 h in 13 Pa (0.1 Torr) of CO_2 gas, and another was stored for 48 h in 2×10^4 Pa (160 Torr) of O_2 gas. The pressures chosen

(23) Wagner, C. D.; Riggs, W. M.; Davis, L. E.; Moulder, J. F.; Muilenberg, G. E. *Handbook of X-ray Photoelectron Spectroscopy*; Perkin-Elmer Corporation: Eden Prairie, 1979.

are consistent with atmospheric partial pressures of the respective gases. Following the allotted storage time, the chamber was pumped down to UHV and the samples were examined for evidence of oxidation using STM, XPS, or both. In all three cases there was no evidence of oxidation. We conclude, therefore, that ozone is the primary cause of the observed monolayer oxidation and that the adventitious ozone vessel contaminants are relatively unreactive to alkanethiol monolayers. We cannot preclude reactions among the contaminants. For example, ozone and water react to form hydroxyl radical.[24,25] This reaction, however, is believed to require ultraviolet photons[24,25] which do not pass through the windows of our UHV chamber.

To determine the reaction site and the molecular scale structural changes accompanying ozone-induced oxidation, STM was conducted at intervals during controlled exposure of the monolayer to the ozone vessel headspace. Figure 3A shows a monolayer prepared by solution deposition and exposed to air for less than 15 min during transfer into the UHV chamber. The surface comprises ~100 Å wide domains of the $c(3 \times 2\sqrt{3})$ crystalline lattice of decanethiol,[1,21,26] a domain boundary network,[1,27−29] and single-atom deep Au vacancy islands (indicated by arrows).[30,31] In some cases the domain boundaries are twins of infinitesimal width, and in other cases they are rotational, translational, or tilt boundaries of molecular width.[1] Exposure of the surface to 4×10^{-5} Pa (3×10^{-7} Torr) of the ozone vessel headspace for 8 min[32] results in a broadening of the boundaries between $c(3 \times 2\sqrt{3})$ domains and concomitant formation of linear features in the resulting regions (See Figure 3B and 4A). Figure 3C shows that continued exposure results in further lateral growth of these linear features at the expense of the $c(3 \times 2\sqrt{3})$ domains. From our observation that the domain boundaries broaden, we infer that they are the nucleation site of the reaction between ozone and decanethiolate monolayers.

A high-resolution image (Figure 4B) and cross-sectional profile (Figure 4E) show that the linear features have a row spacing of 21.5 Å. This row spacing lies within experimental error of the 21.6 Å row spacing previously measured for the δ-phase of decanethiol monolayers on Au(111). The detailed molecular arrangement of the δ-phase is described in ref 21; for the purpose of this paper, we provide a brief description. The δ phase is a striped phase whose areal density is lower than the dense-packed upright phase. It is one of a family of structures that exist for decanethiol below saturation coverage and in which the axes of the hydrocarbon chains are aligned parallel to the surface, rather than away from the surface. At thermodynamic equilibrium, the δ phase coexists with the $c(3 \times 2\sqrt{3})$ at surface coverages where the average molecular area lies between (54.0 and 21.6 Å^2)/molecule.[21] Observation of this row spacing may therefore indicate that the initial reaction product of thiolate with ozone desorbs from the surface, as a result of steric hindrance, leaving behind a subsaturation coverage of decanethiolate with δ and ϕ phases coexisting. The equivalence of the observed row-spacing does not unambiguously identify this current striped phase as δ phase; it is also possible that this phase is due to a packing arrangement of partially oxidized thiols.

Above a threshold ozone exposure, a significant fraction of the near surface region converts to a fluid. We refer to this phase as a fluid because periodic order was not observed in any of the nine repetitions of the experiment. This melting transition occurs on a time-scale faster than the STM image acquisition; therefore, we have not been able to capture it in progress with STM. Figure 3D was captured just above this threshold exposure and from nominally the same surface region as Figure 3C (overlayed line segments indicate corresponding constellation of vacancy islands). The surface is dominated by the 2-dimensional fluid phase and exhibits domains of the phase characterized by 21.5 Å periodic rows (black arrow), a phase characterized by more closely spaced periodic rows (white arrows), the thiolate phase with a $c(3 \times 2\sqrt{3})$ unit cell (pointing fingers), and Au vacancy islands.

The closely spaced striped phase appears at a higher ozone exposure than the 21.5 Å striped phase. Figure 4C shows a molecular-resolution topograph of the closely spaced striped phase. The rows are aligned with substrate ⟨121⟩ directions, have a 5 Å corrugation periodicity (see Figure 4F) and an inter-row spacing of 14.5 Å (see Figure 4G). Indexed to the underlying Au lattice, these directions and spacings are consistent with a primitive rectangular $(5 \times \sqrt{3})$ unit cell (unit cell overlayed in Figure 4C). A recent study from this laboratory characterized all of the structural phases for decanethiol on Au(111).[21] None of the observed phases has a unit cell of $(5 \times \sqrt{3})$; therefore, it is reasonable to assume that the molecules in the $p(5 \times \sqrt{3})$ phase are oxidized thiols. Another recent study characterized the structure of microcontact printed dodecanethiol monolayers.[33] This study reported a $(5 \times \sqrt{3})$ unit cell; however, this study was conducted in an air-ambient, rather than UHV, and therefore it is possible that the observed phase was due to oxidized thiols. The pattern of features in Figure 4C is consistent with a simple rectangular molecular packing with 2 molecules per unit cell. The packing density of the $p(5 \times \sqrt{3})$ is $^3/_5$ that of the $c(3 \times 2\sqrt{3})$ thiolate lattice (ovals overlayed in Figure 4C represent oxidized thiols). Because the $c(3 \times 2\sqrt{3})$ thiolate phase is the densest known phase of decanethiol on Au(111), it is reasonable to infer that some fraction of the thiol molecules desorb when the monolayer undergoes ozone-induced oxidation.[12,13]

Exposing a surface such as that shown in Figure 3D or 4C to the ozone vessel headspace results in complete conversion of the near-surface region to a fluid phase, as shown in Figure 3E. Continued exposure to ozone results in formation of a distribution of raised island features, as indicated by white arrows in Figure 3F, a concomitant diminution of the number and size of the Au vacancy islands, and retention of a fluid surface topography. Figure 4D was acquired from a decanethiol

(24) Ravishankara, A. R.; Hancock, G.; Kawasaki, M.; Matsumi, Y. *Science* **1998**, *280*, 60−61.
(25) Krol, M.; Leeuwen, P. J. v.; Lelieveld, J. *J. Geophys. Res.* **1998**, *103*, 10697−10711.
(26) Camillone, N.; Chidsey, C. E. D.; Liu, G.-y.; Scoles, G. *J. Chem. Phys.* **1993**, *98*, 3503−3511.
(27) Poirier, G. E.; Tarlov, M. J. *Langmuir* **1994**, *10*, 2853−2856.
(28) Delamarche, E.; Michel, B.; Gerber, C.; Anselmetti, D.; Guntherodt, H.-J.; Wolf, H.; Ringsdorf, H. *Langmuir* **1994**, *10*, 2869−2871.
(29) Schonenberger, C.; Jorritsma, J.; Sondag-Huethorst, J. A. M.; Fokkink, L. G. J. *J. Phys. Chem.* **1995**, *99*, 3259−3271.
(30) Edinger, K.; Golzhauser, A.; Demota, K.; Woll, C.; Grunze, M. *Langmuir* **1993**, *9*, 4−8.
(31) Poirier, G. E. *Langmuir* **1997**, *13*, 2019.
(32) In the course of these experiments it was noted that the extent of oxidation, as judged by morphological change, was lesser in the area immediately below the tip and greater in areas several μm removed from the position of the tip during the dose. From this observation we infer that the surface region immediately below the tip apex is shadowed from the ozone flux and that, for experiments in which samples were repetitively dosed and imaged in the same surface region, the extent of morphological change in the images is somewhat less than would have occurred for the same exposure in the absence of the tip.

(33) Larsen, N. B.; Biebuyck, H.; Delamarche, E.; Michel, B. *J. Am. Chem. Soc.* **1997**, *119*, 3017−3026.

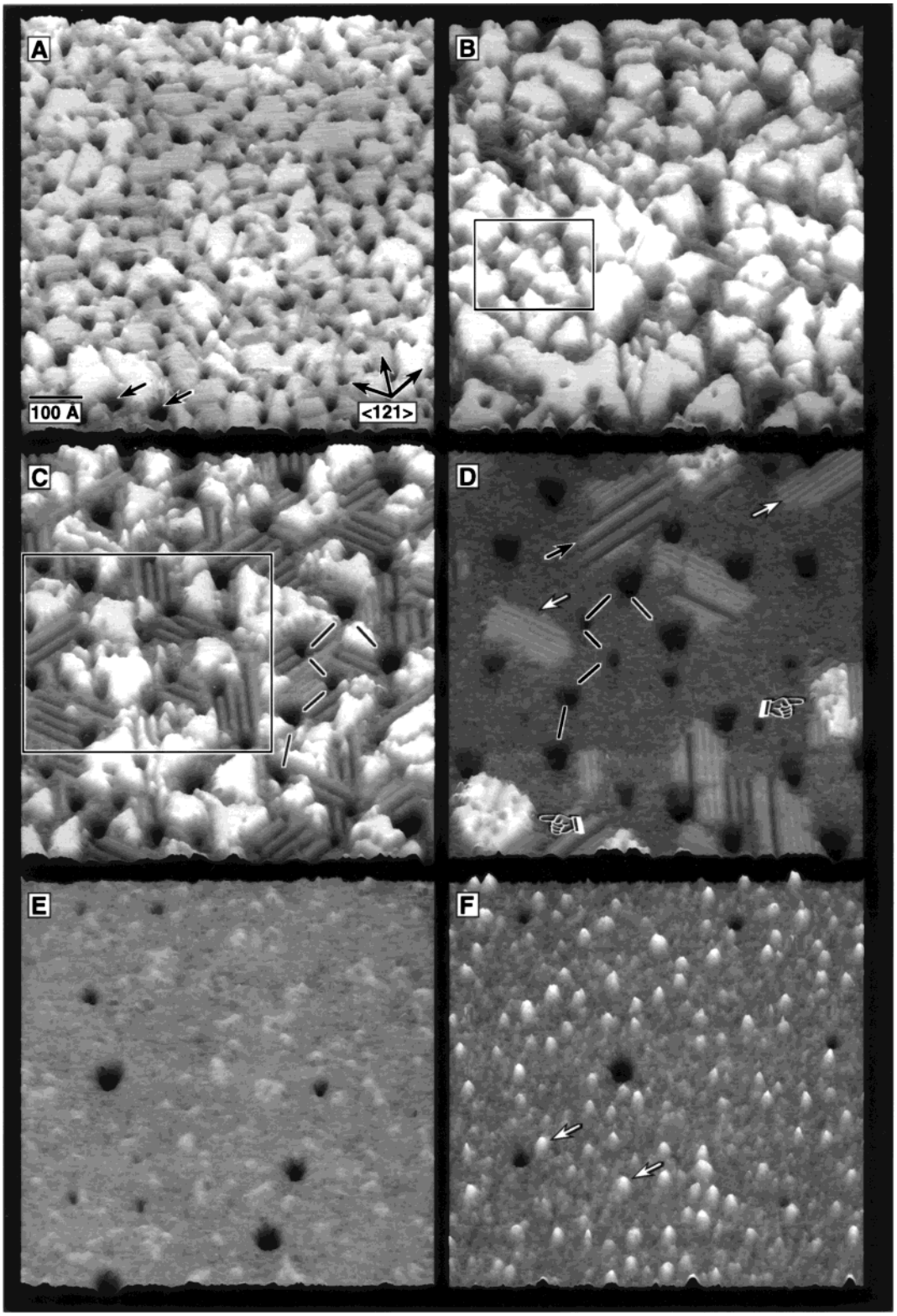

Figure 3. Constant-current UHV STM topographs showing structural evolution of decanethiol monolayers exposed to ozone vessel headspace. Frames B, C, and D were acquired from nominally the same region of the same sample (less than 300 Å drift between image frames); frames A, E, and F were acquired from different samples, but the topography is representative. (A) Topograph of decanethiol monolayer exposed to laboratory air for less than 15 min. Arrows indicate Au vacancy islands. Scale bar and crystallographic azimuths apply also to B through F. (B) Topograph of decanethiol monolayer exposed to 10^{-5} Pa (10^{-7} Torr) of ozone vessel headspace for 8 min. Region indicated by rectangle is shown at higher magnification in Figure 4A. (C) Topograph of decanethiol monolayer exposed to 10^{-5} Pa (10^{-7} Torr) of ozone vessel headspace for 27 min.[32] Region indicated by rectangle is shown at higher magnification in Figure 4B. (D) Topograph of decanethiol monolayer exposed to 10^{-5} Pa (10^{-7} Torr) of ozone vessel headspace for 33 min.[32] Line segments indicate constellation of vacancy islands corresponding to those in C, black arrow indicates 21.5 Å period stripe features, white arrows indicate 14.5 Å period stripe features, pointing fingers indicate residual $c(3 \times 2\sqrt{3})$ thiolate domains. (E) Additional exposure to ozone vessel headspace results in complete conversion to a fluid surface phase. (F) Additional exposure to ozone results in formation of Au island features (arrows).

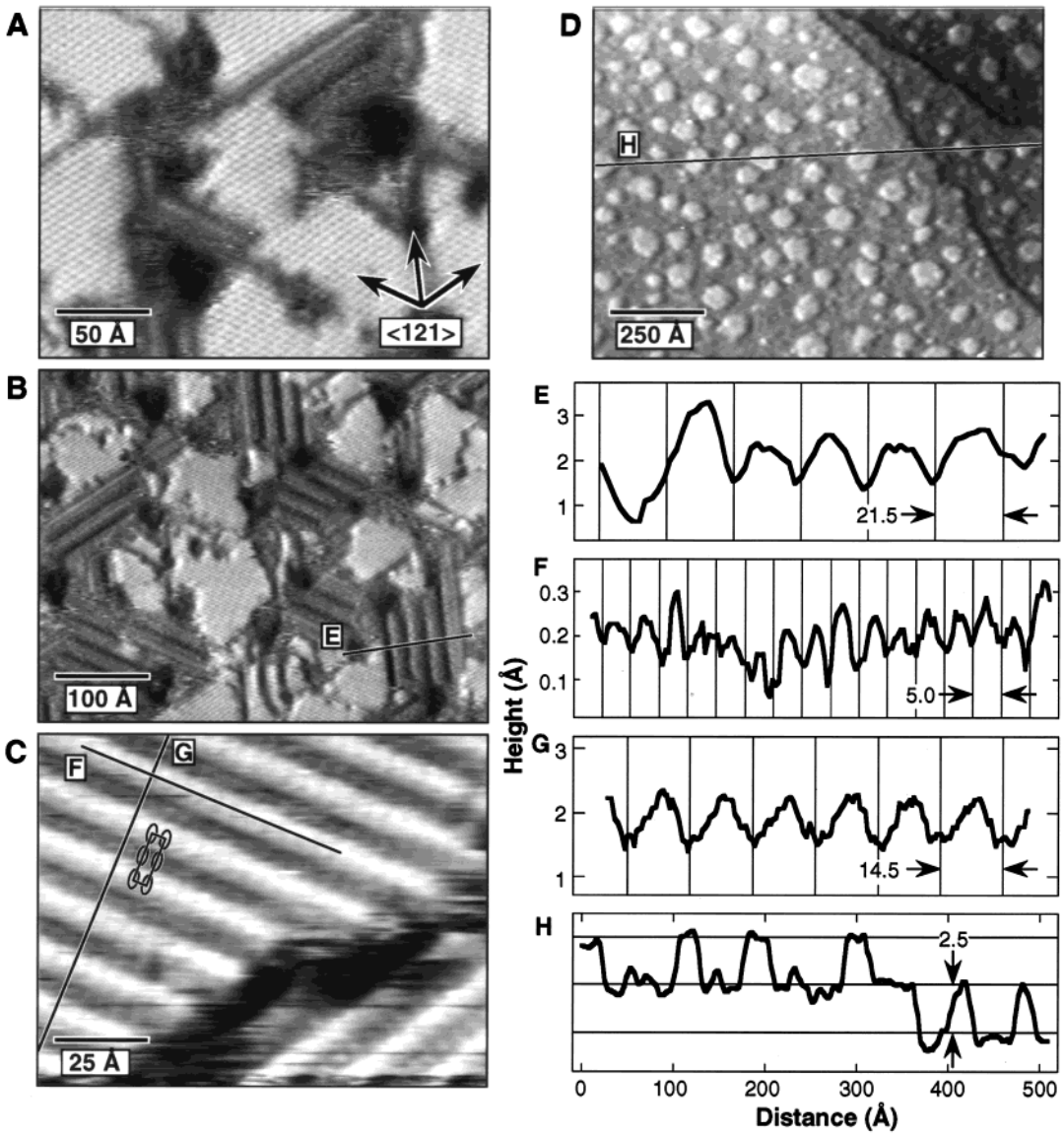

Figure 4. High-resolution constant-current UHV STM topographs at intermediate stages of oxidation along with cross-sectional height profiles of salient features. To enhance contrast, frames A, B, and D are represented as a summation of the topograph and the derivative of the topograph. (A) STM topograph acquired from corresponding region in Figure 3B showing initial conversion of domain boundary network to striped phase. (B) STM topograph acquired from corresponding region in Figure 3C showing lateral growth of striped phase. (C) Molecular resolution topograph of stable crystalline, commensurate phase indicated by white arrows in Figure 3D. Overlayed ovals represent likely position of oxidized thiols, overlayed rectangle represents $p(5\text{x}\sqrt{3})$ unit cell. (D) Topograph of decanethiol monolayer exposed to laboratory air for 1 day showing distribution of island features comparable to Figure 3F. (E) Cross-sectional height profile from corresponding line segment in part B shows 21.5 Å repeat period of initial striped phase. (F) Cross-sectional height profile from corresponding line segment in part C shows 5 Å corrugation periodicity of second striped phase. (G) Cross-sectional height profile from corresponding line segment in part C shows 14.5 Å row period of second striped phase. (H) Cross-sectional height profile from corresponding line segment in part D shows 2.5 Å height of island features and equivalence to Au single-atom step height.

monolayer exposed to laboratory air for 1 day and shows a similar distribution of island features as seen in Figure 3F. Cross-sectional profiles (see Figure 4H) show that the height of these island features is indistinguishable from that of a Au single-atom step. The height of these protrusions was found to depend neither on tunneling bias voltage nor on set point current, indicating that they are not chemically different than the terrace. We conclude, therefore, that these features are Au islands and that the Au islands and Au terraces are uniformly covered by a fluid phase of oxidized alkanethiol monolayer.

Because it is buried under an amorphous oxidized amphiphile monolayer, it is difficult for us to discern whether the interface Au layer is crystalline or amorphous. In either case, diminution of the Au vacancy islands and appearance of the Au islands are both indicative of expansion of the mean Au atom spacing in the Au surface layer.[34,35] Height histograms from five repetitions of the experiment showed that the island fraction varied between 5 and 20% of a monolayer. Taking into account that the nascent thiolate monolayers exhibit vacancy islands the coverage of which varies between 5 and 10%,[31] we conclude that the islands arise because the Au layer at the oxidized thiol interface is expanded relative to the bulk (111) layers by 10−30%.

Background experiments were conducted to confirm that the chemical and structural changes that we observe were not due

(34) Poirier, G. E. *J. Vac. Sci. Technol. B* **1996**, *14*, 1453−1460.
(35) Barth, J. V.; Schuster, R.; Behm, R. J.; Ertl, G. *Surf. Sci.* **1994**, *302*, 158−170.

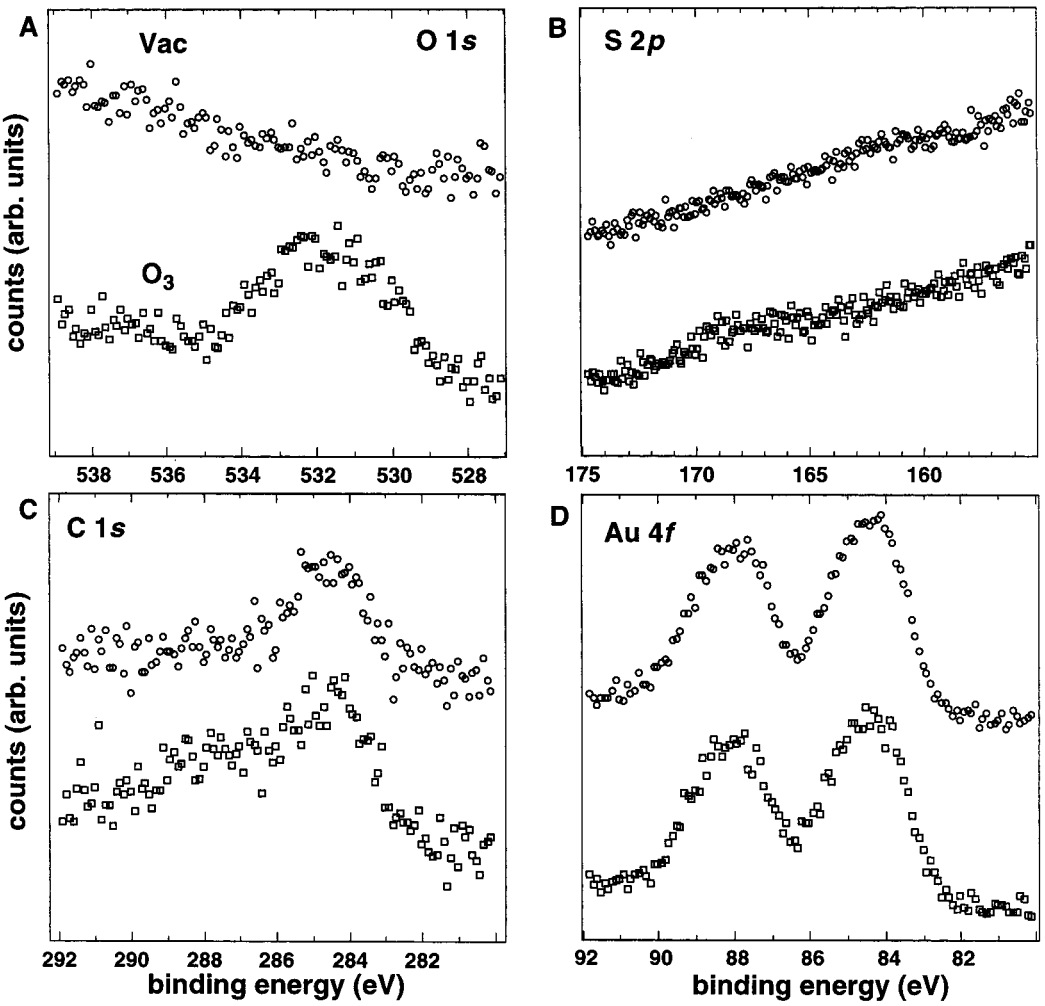

Figure 5. X-ray photoelectron spectra of Au(111) herringbone surface before and after exposure to ozone. Spectra in open circles are from sample prepared by sputtering and annealing in UHV (labeled "vac" in A), spectra in open squares were acquired after exposing this sample to 2×10^{-6} Torr of ozone Dewar headspace for 37 min (labeled "O_3" in A). (A) Spectra in O 1*s* region shows that exposure results in adsorption of oxygen. (B) Spectra in S 2*p* region shows insignificant adsorption of sulfur. (C) Spectra in C 1*s* region shows contamination on cleaned surface and modest increase after exposure. (D) Spectra in Au 4*f* region shows that exposure results in modest decrease of Au photoemission and no detectable broadening.

to, say, complete desorption of the monolayer and replacement by species in the ozone Dewar headspace. The chemistry and structure of the Au surface were determined using XPS and STM before and after exposure to the ozone Dewar headspace. The spectrometer settings used for the spectra in Figure 5 are unchanged from those used for the spectra in Figure 2. Figure 5A shows that exposure of the bare Au surface to ozone results in appearance of a broad photoemission peak in the O 1*s* region,[36] Figure 5B shows less than detectable sulfur, both before and after exposure, Figure 5C shows residual carbon photoemission after sputtering and annealing, and a modest increase after exposure, and Figure 5D shows a modest attenuation of the Au 4*f* photoemission following exposure. The results in Figure 5 thus indicate, consistent with prior reports in the literature,[22,36] that ozone exposure results in deposition of a significant amount of oxygen, and a small amount of carbon. This contrasts the result shown in Figure 2, where we observed retention of significant S 2*p* and C 1*s* photoemission in monolayers exposed to the ozone Dewar headspace. From this we conclude that the alkanethiol monolayers are not completely displaced by species from the ozone Dewar headspace and the features that we observe in Figures 3 and 4 are due to an oxidized thiol monolayer.

Figure 6 shows the effect of ozone exposure on the structure of the Au surface. Prior to exposure, the surface exhibits the characteristic herringbone reconstruction (Figure 6A).[37] Residual carbon contamination (see Figure 5C) results in perturbation of the herringbone ridges adjacent to the step edge in the lower part of the topograph. Adsorption of surface oxygen, induced by exposure to ozone, results in lifting of the herringbone reconstruction, disordering of the surface layer, and formation of Au island features. The island features in Figure 3F and 4D, and those shown in Figure 6B, are in each case caused by expansion of the Au surface layer and ejection of the excess atoms onto the terrace level. For the case of thiolate monolayers, Au atoms at the Au-thiolate interface have the bulk in-plane lattice constant.[1,26,27,38] Exposure to ozone results in expansion of the atomic spacing at the Au interface to a value greater than the bulk spacing. For the case of bare Au surfaces, Au atoms in the herringbone reconstruction adopt a 4.5% contracted lattice relative to the bulk.[37,39] Exposure to ozone lifts this reconstruction, expanding the surface Au atom density to the bulk value,

(36) King, D. E. *J. Vac. Sci. Technol. A* **1995**, *13*, 1247−1253.

(37) Chambliss, D. D.; Wilson, R. J.; Chiang, S. *J. Vac. Sci. Technol. B* **1991**, *9*, 933−937.

(38) Fenter, P.; Eisenberger, P.; Li, J.; Camillone, N.; Bernasek, S.; Scoles, G.; Ramanarayanan, T. A.; Liang, K. S. *Langmuir* **1991**, *7*, 2013−2016.

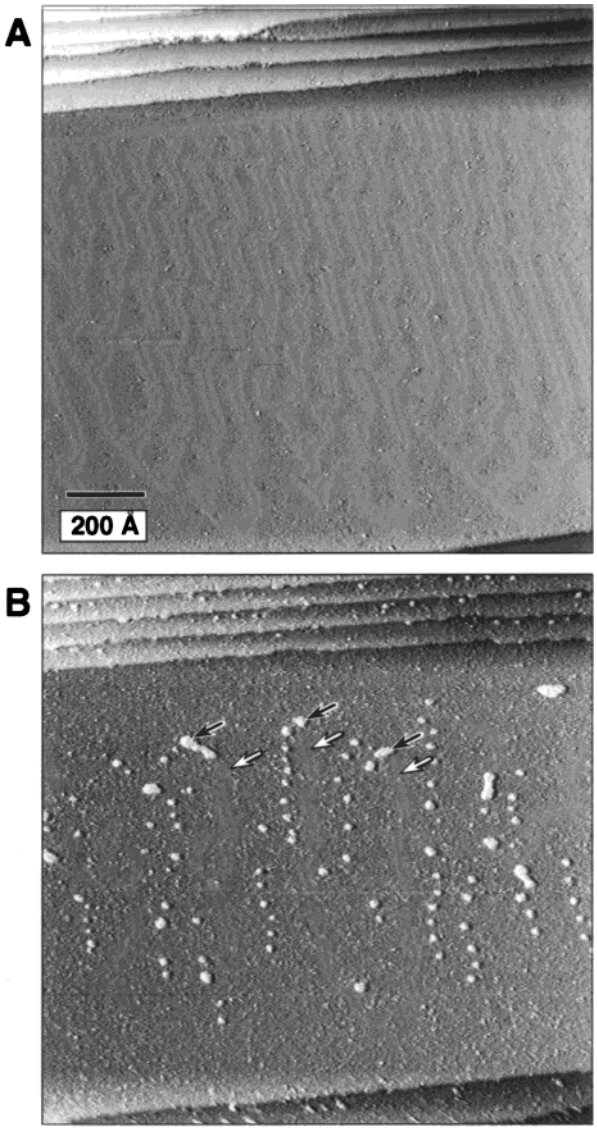

Figure 6. Constant-current UHV STM topographs showing morphological change of Au(111) herringbone reconstruction after exposure to ozone vessel headspace. Data are shown as summation of height and height gradient. (A) Herringbone reconstructed Au(111), horizontal features in lower and upper region of image are single atom steps. Carbon contamination perturbs herringbone ridges adjacent to step edge in lower part of topograph. (B) Exposure to 3×10^{-7} Torr of ozone Dewar headspace for 15 s. results in lifting of herringbone reconstruction (white arrows indicate remaining ridges), creation of Au island features (indicated by black arrows), and formation of fluid surface topography. Exposure for additional 21 min did not alter island features but resulted in removal of remnant herringbone ridges.

and concomitantly forming ~4.5% monolayer of Au islands. Similar islands were observed by Tao and Lindsay on surfaces where the herringbone reconstruction was electrochemically lifted.[40]

The mechanistic pathway of monolayer oxidation is shown in Scheme 1. Scheme 1A represents the thiolate monolayer comprising domains of the $c(3 \times 2\sqrt{3})$ unit mesh[26,27] separated by molecular-width domain boundaries.[27] Controlled exposure to ozone results in oxidation of the thiolates at the domain boundaries and a concomitant conversion to a striped packing arrangement (Scheme 1B). This first striped phase may

Scheme 1. Sequence of Structural Changes that Accompany Ozone-Induced Oxidation of Decanethiol Monolayer on Au(111)[a]

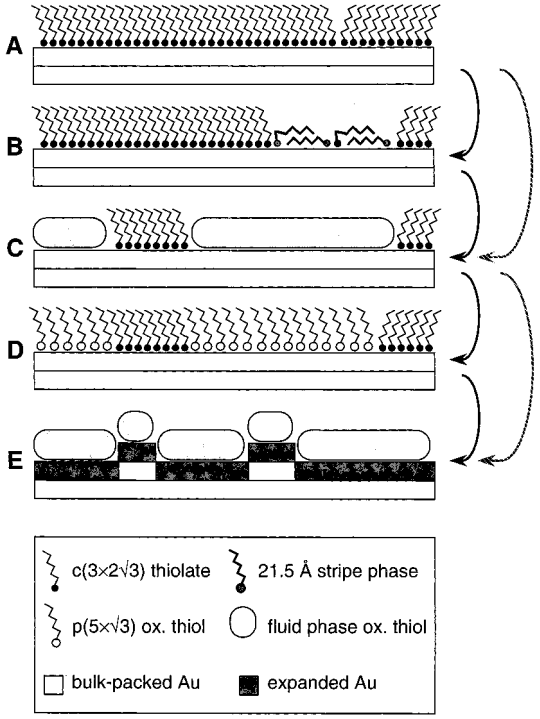

[a] See text for descriptions of A−E.

be due to δ-phase decanethiolate or it may be assignable to a phase of oxidized decanethiol. Additional exposure of the surface to ozone results in conversion of the surface layer to a fluid phase. This fluid phase may be pure thiolate or it may be a mixture of oxidized and reduced thiols (Scheme 1C). If allowed to evolve in a vacuum for several hours, this fluid will recrystallize into a commensurate phase with a $p(5 \times \sqrt{3})$ unit mesh (Scheme 1D). It is reasonable to infer that this $p(5 \times \sqrt{3})$ phase comprises partially oxidized thiols. If the surface schematized in 1C or in 1D is exposed to additional ozone, the entire surface fluidizes and the Au at the monolayer−Au interface expands by 10−30% resulting in a two-tiered surface uniformly covered with an amorphous, oxidized thiol monolayer (Scheme 1E). The solid arrows indicate the progression of phases if the oxidation is carried out slowly, under conditions close to equilibrium, the dashed arrows indicate the progression of phases under rapid oxidation. Monolayers oxidized by ozone in UHV and stored in UHV for up to 3 days did not show significant morphological change from the amorphous islanded surface structure. Monolayers oxidized in air for up to 4 days likewise retained the amorphous islanded surface structure but the number density of Au islands increased.

Conclusions

This study revealed molecular-scale features associated with the reaction of ozone with decanethiol monolayers. The reaction initiates at the domain boundary network of the alkanethiol monolayer and propagates into the domains. The reacted monolayer exhibits two striped phases prior to the final oxidized monolayer structure. The initial striped phase has a row-spacing of 21.5 Å; at higher ozone exposure a second striped phase forms that has a row-spacing of 14.5 Å. The unit-cell dimensions of the second striped phase are consistent with a primitive $(5 \times \sqrt{3})$ mesh and the pattern of protrusions suggests a

(39) Sandy, A. R.; Mochrie, S. G. J.; Zehner, D. M.; Huang, K. G.; Gibbs, D. *Phys. Rev. B* **1991**, *43*, 4667−4687.
(40) Tao, N. J.; Lindsay, S. M. *J. Appl. Phys.* **1991**, *70*, 5141−5143.

packing density that is $^3/_5$ that of the dense-packed thiolate monolayer. From this we infer that a fraction of the alkanethiol molecules desorb as a result of oxidation. The fully oxidized monolayer is not crystalline; rather, it is amorphous, and is supported on an expanded Au surface layer. The insight provided by these studies may be used to guide efforts aimed at creating more robust monolayers and to design storage protocols that prevent or inhibit air oxidation of alkanethiol monolayers.

Acknowledgment. G.E.P. is grateful for helpful discussions with R. F. Huie and J. E. Norris in the early stage of these studies.

JA991739F